Macromolecules

ARTICLE

pubs.acs.org/Macromolecules

Dielectric study of Poly(styrene-*co*-butadiene) Composites with Carbon Black, Silica, and Nanoclay

Loan T. Vo,[†] Spiros H. Anastasiadis,[‡,§] and Emmanuel P. Giannelis[†,*]

[†]Department of Materials Science and Engineering, Cornell University, Bard Hall, Ithaca, New York 14853, United States

[‡]Institute of Electronic Structure and Laser, Foundation for Research and Technology—Hellas, P.O. Box 1527, 711 10 Heraklion Crete, Greece

[§]Department of Chemistry, University of Crete, 710 03 Heraklion Crete, Greece

Supporting Information

ABSTRACT: Dielectric spectroscopy is used to measure polymer relaxation in styrene−butadiene rubber (SBR) composites. In addition to the bulk polymer relaxation, the SBR nanocomposites also exhibit a slower relaxation attributed to polymer relaxation at the polymer−nanoparticle interface. The glass transition temperature associated with the slower relaxation is used as a way to quantify the interaction strength between the polymer and the surface. Comparisons were made among composites containing nanoclay, silica, and carbon black. The interfacial relaxation glass transition temperature of SBR−clay nanocomposites is more than 80 °C higher than the SBR bulk glass transition temperature. An interfacial mode was also observed for SBR−silica nanocomposites, but the interfacial glass transition temperature of SBR−silica nanocomposite is somewhat lower than that of clay nanocomposites. An interfacial mode is also seen in the carbon black filled system, but the signal is too weak to analyze quantitatively. The interfacial polymer relaxation in SBR−clay nanocomposites is stronger compared to both SBR−carbon black and SBR−silica composites indicating a stronger interfacial interaction in the nanocomposites containing clay. These results are consistent with dynamic shear rheology and dynamic mechanical analysis measurements showing a more pronounced reinforcement for the clay nanocomposites. Comparisons were also made among clay nanocomposites using different SBRs of varying styrene concentration and architecture. The interfacial glass transition temperature of SBR−clay nanocomposites increases as the amount of styrene in SBR increases indicating that styrene interacts more strongly than butadiene with clay.

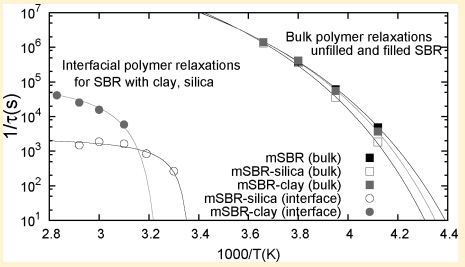

INTRODUCTION

Styrene−butadiene rubber (SBR) is used extensively in industry and is often further enhanced by adding fillers. Carbon black has been the filler of choice due to its low cost, but carbon black makes the material black (which is undesirable in certain applications) and a large amount of carbon black is needed to achieve the desired properties. There have been efforts to replace carbon black with other fillers such as precipitated silica,[1] inorganic fibers,[2] organic whiskers,[3] carbon nanotubes,[4] and layered silicate clays.[5−11] In this study, we compare SBR composites with carbon black, silica, and organically modified montmorillonite clay (nanoclay), with the focus on SBR−clay nanocomposites. Clay at a concentration of 10 phr in natural rubber has been demonstrated by Okada et al. as having comparable tensile properties to 40 phr of carbon black.[7]

Reinforcement in filled elastomers is not well understood but is generally attributed to the interactions between the added particles and rubber. The existence of a glassy layer at the particle−rubber interface due to the interactions between the particles and the rubber has been suggested[12] to explain early NMR results[13] and mechanical[14−17] data. Given the possible nanoscale dimensions and high surface to volume ratio of the added particles, the glassy interphase can comprise a large fraction of the composite and can strongly influence the mechanical properties of the composite.[18−20] In thin polymer films on inorganic substrates, the existence of slow dynamics and, thus, an effective glass transition, T_g, increasing with decreasing film thickness has been attributed to the existence of attractive interaction between the polymer and the substrate.[21,22] On the other hand, the bulk of the data on the effective glass transition of thin films weakly interacting with the underlying substrate agree with significant T_g reductions.[23,24] It is noted that the equivalence in the behavior between polymer nanocomposites and thin polymer films has been quantitatively verified for silica/polystyrene nanocomposites.[25]

Copolymer rubbers, such as SBR, have an added complexity in that there are two polymer components with which filler particles can interact. In polymer blend nanocomposites, if the particles interact favorably with only one polymer, then the particles reside only in that polymer phase.[26] However, with copolymer nanocomposites, if the clay interacts favorably with only one polymer,

Received: January 10, 2011
Revised: June 26, 2011
Published: July 13, 2011

Table 1. Molecular Characteristics of the Styrene and Butadiene Homopolymers and Copolymers of Varying Compositions and Architecture

reference	sample	composition wt % styrene	source	M_w (kg/mol)	M_w/M_n	T_{gb} (°C)
PB	polybutadiene homopolymer	0	Lanxess	175	1.9	−96
SBR5	styrene−butadiene random copolymer	5	Sp[2]	380	3.6	−75
SBR23	styrene−butadiene random copolymer	23	Sp[2]	350	4.6	−63
SBR45	styrene−butadiene random copolymer	45	Sp[2]	547	5.8	−79
PS	polystyrene homopolymer	100	Sigma-Aldrich	192	1.4	107
SB30	polystyrene-*block*- polybutadiene diblock copolymer	30	Sigma-Aldrich	54		−95, 58
mSBR	styrene−butadiene random copolymer	27	Michelin	130	1.7	−48

the nanoparticles can still be dispersed throughout the matrix.[27] Interactions of each polymer component with the added particles will affect nanocomposite processing and properties, so it is crucial that polymer−particle interactions for each polymer component be quantified within a copolymer and not just with homopolymers alone.

As crucial as SBR−filler interactions are to material properties, it is difficult to measure these interactions directly. SBR−filler interactions have been measured indirectly by measuring the amount of SBR adsorption from solvent onto carbon black substrate,[28] the cross-link density of composite compared to unfilled SBR, and the amount of swelling of the composite when added to solvent.[8] More direct measurements of SBR−filler interaction have included using NMR spectroscopy to probe SBR mobility close to carbon black particles.[29−31] The existence of the glassy polymer−particle interfacial layer was indeed shown with NMR measurements whereas the mechanical behavior of the glassy interfacial layer was also measured by DMA.[17,32] In the present investigation, we probe the SBR−particle interfacial layer utilizing broadband dielectric relaxation spectroscopy.

Dielectric spectroscopy measures dipolar relaxation of polymers and is useful in studying polymer dynamics. Dielectric spectroscopy offers a wide range of frequencies and temperatures such that polymer dynamics can be measured over many different time scales. In particular, the segmental or α-relaxation can be measured by dielectric relaxation spectroscopy. The α-relaxation process is related to the local motion of polymer segments, which become increasingly slow as the glass transition is approached; the glass transition temperature is poorly defined and is conventionally determined as the temperature at which the relaxation time of the segmental relaxation, τ, is, e.g., 100 s, an arbitrarily long time. Dielectric spectroscopy measures the relaxation times at several temperatures, and T_g can be estimated from the temperature dependence of the relaxation.

In this study, in addition to the bulk segmental relaxation responsible for the bulk T_g, dielectric relaxation spectroscopy also showed a second, slower segmental relaxation mode in all SBR−composite samples. We attribute this slower relaxation mode to the reduced mobility of SBR at the interface—segments which are adsorbed on the surface of the nanoadditives due to attractive interactions. The effective glass transition temperature associated with this slower relaxation, T_{gi} (interfacial glass transition temperature), is more than 80 °C higher than the bulk glass transition temperature, T_{gb}. We have also used the estimated interfacial glass transition temperature together with the obtained dielectric strength of the interfacial relaxation process as a means to quantify the interaction strength between the polymers and the added nanoparticles. The interaction strength between SBR and different fillers increases as carbon black ≤ silica < clay. Lastly, we compare the interactions of two different clays with SBRs of varying styrene content and structure. The comparisons show that SBR interacts most strongly with nanoclay and that the styrene component of SBR is responsible for the strongest interactions.

Table 2. Characteristics of Mixes of SBR with Curing Agents and Additives

sample	20A clay	silica	carbon black	curing agents?	cured?
mSBR−20A	5 phr	0	0	yes	no
mSBR−silica	0	5 phr	0	yes	no
mSBR−CB	0	0	5 phr	yes	no

EXPERIMENTAL PART

Materials. For the studies involving copolymers of different compositions, the styrene−butadiene rubber (SBR) random copolymers were provided by Lanxess or obtained from various sources as listed in Table 1. All copolymers contain at least 50% butadiene to ensure good dielectric signal as styrene dielectric signal is weak. Also included in Table 1 are the characteristics of a polystyrene-*block*-polybutadiene diblock copolymer that was studied for comparison.

All copolymers were processed similarly. The polymers were ground to 1 mm particles, mixed with the appropriate amount of clay in a speed mixer, pressed into 20 mm diameter, 1 mm thick disks at room temperature with a load of 150 MPa, and annealed in a vacuum oven above the T_g of the polymer (130 °C for SBR composites) for 24 h.

For the studies involving different fillers, an SBR provided by Michelin containing 27% styrene by weight, mSBR, was used. Composites with mSBR were prepared at Michelin. Cured, uncured (but containing curatives), and uncured (with no curatives) were analyzed. Curatives include 2 phr zinc oxide, 2 parts SAD stearic acid, 1.5 parts sulfur, and 1.5 parts CBS, a sulfonamide based accelerator. For analysis, disks were cut from these samples. The sample names and mix components are listed in Table 2. In addition to the components listed in Table 2, it should be noted that there are no silica coupling agents in the mSBR−silica mix.

Modified montmorillonite clays (Cloisite 93A and Cloisite 20A) were obtained from Southern Clay Products. Cloisite 20A (herein referred to as C20A) is modified with dimethyl dehydrogenated ditallow alkyl ammonium and intercalates both polystyrene and polybutadiene. Cloisite 93A (herein referred to as C93A), modified with methyl dehydrogenated ditallow alkyl ammonium is less polar than C20A and intercalates polybutadiene homopolymer but not polystyrene. The clay powders were used as received. For dielectric studies, the clay amount was less than 5% by weight (to minimize complications from clay conductivity), and the pellets were annealed until complete intercalation was observed

dx.doi.org/10.1021/ma200044c |*Macromolecules* 2011, 44, 6162–6171

via X-ray diffraction. The silica and carbon black samples were provided by Michelin. The BET surface areas for C20A, silica and carbon black are 10, 160, and 30 m^2/g, respectively. For consistency, all samples were processed similarly. Well-dispersed and, in the case of clay, intercalated nanocomposites were obtained for all samples (see figures in Supporting Information).

Experimental Methods. Structural characterization of the clay nanocomposites was performed with X-ray diffraction, using a Scintag Inc. $\theta-\theta$ diffractometer. The CuKα radiation was used with wavelength $\lambda_{CuK\alpha}$ = 1.54 Å. A germanium detector was utilized with a scanning rate of 3°/min.

Bulk glass transition temperatures were measured with differential scanning calorimetry (DSC) using a TA Instruments Q1000 DSC scanning at 10 °C/min.

Polymer relaxation was measured using dielectric spectroscopy with a Novocontrol N40 broadband spectrometer. Pellets of the annealed composite were placed between parallel gold plated electrodes 20 mm (top) and 30 mm (bottom) in diameter. Measurements swept through a frequency, f, range of 1 Hz to 10^6 Hz at isothermal conditions that varied from −100 to +140 °C.

The rheological properties of the nanocomposites were determined using a Paar Physica Modular Compact Rheometer 300 (MCR 300) equipped with parallel plate geometry (diameter 25 mm). Small amplitude oscillatory shear measurements were performed in a dry nitrogen atmosphere to suppress oxidative degradation. The isothermal frequency scans covered a range of angular frequency (ω) from 0.1 to 300 s^{-1}. Dynamic mechanical analysis (DMA) was carried out on a TA Instruments DMA Q800 using the film/fiber tension clamp. Temperature scans were performed at 1 Hz and a rate of 5 °C/min.

RESULTS AND DISCUSSION

The series of plots in Figure 1 show dielectric relaxations of SBR at different temperature ranges, filled and unfilled. Figure 1a shows the dielectric loss, ε'', spectra as a function of frequency for unfilled mSBR at temperatures approaching its glass transition temperature of −48 °C (Table 1). Each spectrum can be fit to the Havriliak−Negami (HN) function. A typical fit of the dielectric data to the HN function is shown in Figure 1e for T = −20 °C. A characteristic relaxation time, τ, is obtained from the HN fit to each spectrum or a curve fit to the peak maximum frequency. Figure 2 shows some relaxation times plotted as a function of inverse temperature. The relaxation times were obtained from a curve fit to the peak maximum frequency at each temperature. The temperature dependence of the relaxation time is described by the Vogel−Fulcher−Tammann (VFT) equation

$$\tau(T) = \tau_\circ \exp\left(\frac{B}{T - T_\circ}\right) \quad (1)$$

where τ_o, B, and T_0 are constants. By convention T_g is obtained by extrapolating the fit to the temperature at which τ is equal to 100 s. A bulk glass transition temperature, T_{gb}, is calculated for mSBR to be −44 °C, very similar to that measured by DSC (Table 1).

Figure 1b shows the dielectric loss, ε'', spectra for the same polymer (mSBR) at higher temperatures. At these temperatures, the segmental relaxation process associated with the bulk glass transition is fast and thus not within this frequency window. For unfilled SBR, there is no relaxation observed in this temperature range.

In contrast, SBR mixed with clay (mSBR−C20A) displays two segmental relaxation modes: a fast process, which is observed at lower temperatures (Figure 1c) that is attributed to the bulk polymer relaxation, and a slow process observed at higher temperatures (Figure 1d) that is attributed to the interfacial polymer relaxation. At the lower temperature range (−40 to +10 °C), the dielectric loss spectra of the nanocomposite (Figure 1c) appears to be identical to the spectra for the unfilled mSBR polymer (Figure 1a) as shown in Figure 2. Indeed, the dynamics shown in Figure 1 a and c as well as the T_{gb} calculated for the mSBR−C20A nanocomposite is the same as for the unfilled polymer indicating that bulk polymer relaxation is not affected by the addition of nanoparticles (this is true for clay, silica, and carbon black).

However, unlike unfilled SBR, SBR nanocomposites also exhibit a slower relaxation at higher temperatures (20° to 90°) as shown in Figure 1d for the mSBR−C20A clay nanocomposite. This relaxation is different from the faster process that is observed at lower temperatures (Figure 1c). Analysis of the dielectric loss spectra in Figure 1d requires the use of two HN functions together with an ω^{-1} power law conductivity term, which is apparently stronger in the nanocomposites than in unfilled polymers. The slower of the two HN functions is attributed to a Maxwell−Wagner polarization due to the solid interfaces in the specimen whereas the faster of the two processes is related to polymer next to the inorganic surfaces, thereafter referred to as the interfacial process. An example of this fit[33] is shown in Figure 1f for the spectra at 60 °C.

Figure 2 shows the relaxation times of both the bulk mode and the slower interfacial mode plotted as a function of inverse temperature. The solid lines in Figure 2 are fits to the data using the VFT function (eq 1). The parameters for these fits are listed in Table 3. The relaxation times of the interfacial process are by orders of magnitude slower than the ones for the bulk segmental relaxation. An effective "glass transition-like temperature" can be assigned to this slow interfacial relaxation process in analogy to the assignment of a glass transition temperature when the polymer segmental relaxation is considered. For the mSBR−C20A nanocomposite, this effective interfacial glass transition T_{gi} is estimated as 36 °C,[34] i.e., 80 °C higher than the bulk glass transition temperature, T_{gb}. Essentially, the polymer at the polymer−clay interface is "glassy" compared to the surrounding bulk polymer.

Glassy interphase behavior has been observed previously in clay nanocomposites[35−37] as well as with other nanoparticles such as silica;[17,32] the thickness of such a layer has been estimated from experimental results to be between 2 and 9 nm. The existence of slow glassy-like interfacial layers has been attributed to strong attractive interactions between the polymer and the solid surfaces.[21,22] On the other hand, significantly faster dynamics have been observed for free-standing films or for supported films on noninteracting substrates,[23,24,38,39] both controlled by the behavior close to the free surface, as well as for weakly interacting polymers intercalated within inorganic silicate layers in polymer/clay nanocomposites.[40−49] The significantly faster dynamics within the galleries was attributed to the suppression[42,50] of cooperativity[51,52] that inherently slows down the dynamics as the glass transition is approached by decreasing temperature. In the present case, the polymer motion has become significantly slower compared to the bulk. We believe the slower polymer motion measured by dielectric relaxation spectroscopy is likely due to the polymer surrounding the clay stacks and layers in a strongly interacting system.

Because silica nanoparticles are more commonly used with SBR, the segmental relaxation of mSBR−silica was compared to

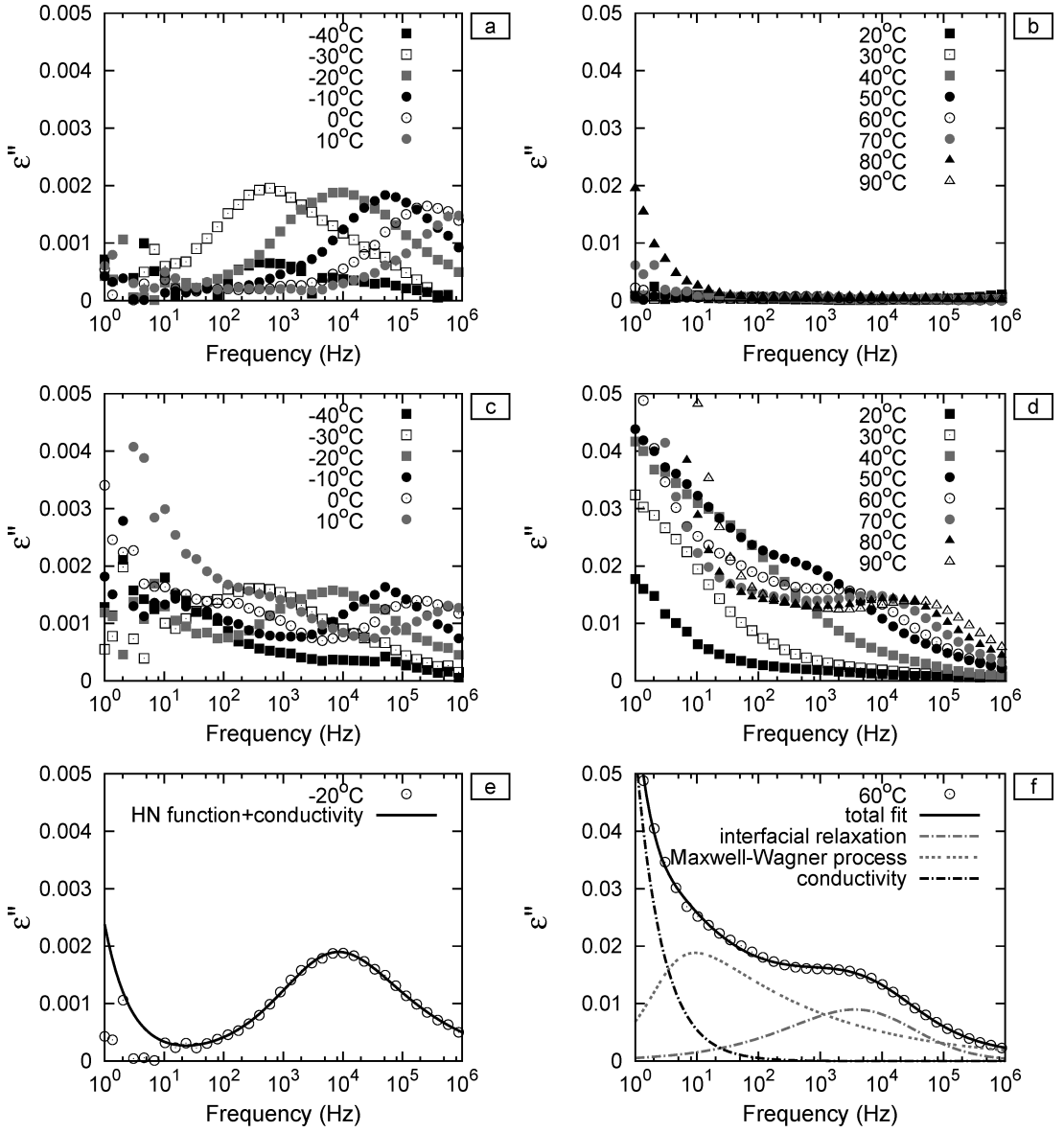

Figure 1. (a) Dielectric loss, ε'', spectra of mSBR at temperatures ranging from −40 to +10 °C. (b) Dielectric loss, ε'', spectra of mSBR at temperatures ranging from 20 to 90 °C showing that there are no slower relaxations for unfilled mSBR. (c) Dielectric loss, ε'', spectra of mSBR−C20A clay nanocomposite at temperatures ranging from −40 to +10 °C. Nanocomposite dielectric loss spectra at these temperatures appear similar to unfilled mSBR dielectric loss spectra (a). (d) Dielectric loss, ε'', spectra of mSBR−C20A at temperatures ranging from 20 to 90 °C. Higher temperature relaxations in the same frequency range indicate a slower polymer relaxation. (e) Dielectric loss spectrum for unfilled mSBR at $T = -20$ °C. Black solid line is the fit to the sum of the HN equation and a power law function with exponent −1 for the conductivity. (f) Dielectric loss spectrum for mSBR−20A clay nanocomposite at $T = 60$ °C. Black solid line is the total fit to the sum of a HN function for the interfacial polymer relaxation, a HN function for the Maxwell−Wagner polarization, and a power law function with exponent −1 for the conductivity. Dashed lines are individual components to the total fit.

that of mSBR−C20A. Similar to clay nanocomposites, a slower relaxation was observed in the silica nanocomposites as well. However, the temperature dependence of the slower relaxation attributed to the interfacial polymer in the two composites is different as shown in Figure 2. The effective glass transition of the interfacial polymer for mSBR−silica nanocomposite occurs at a somewhat lower temperature (T_{gi} = 22 °C) than that for mSBR−20A clay nanocomposite (T_{gi} = 36°C). T_{gi} is a measure of the dynamics of the polymer interacting with the nanoparticle; thus, the interfacial polymer in the clay nanocomposite is slower than that of the polymer in the silica nanocomposite. The slower dynamics might be indicative of stronger interactions in the clay nanocomposites. Silica contains hydroxyl groups on the surface which interact differently with SBR compared to the oxygen atoms in the clay layers.

The primary additive used with SBR in industry is carbon black. A major application of SBR is in tires, and tires are generally formulated with a large (>30%) amount of carbon black to improve various properties. We have used dielectric spectroscopy to probe SBR samples filled with carbon black (CB) in an attempt to quantify the SBR−CB interactions. Carbon black is conductive, and the signal from the conductivity can mask the signal from the polymer relaxation. To circumvent this effect, the concentration of carbon black is kept very low (at 5 phr) relative

dx.doi.org/10.1021/ma200044c |*Macromolecules* 2011, 44, 6162–6171

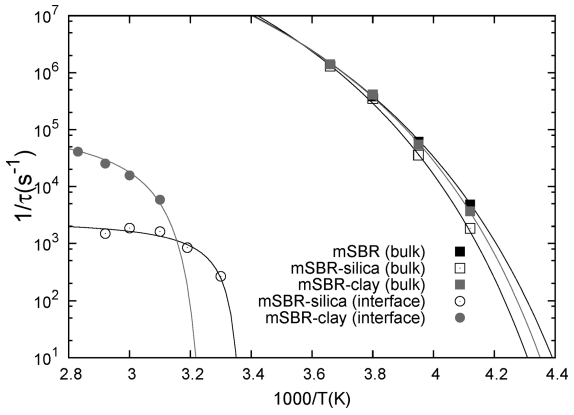

Figure 2. Bulk and interfacial relaxation times as a function of temperature for mSBR and mSBR nanocomposites with C20A clay and silica. Lines are VFT (eq 1) fits to the data. The extrapolated interfacial glass transition temperatures, T_{gi}, for mSBR, mSBR−C20A, and SBR−silica nanocomposites are −44, +36, and +22 °C, respectively.

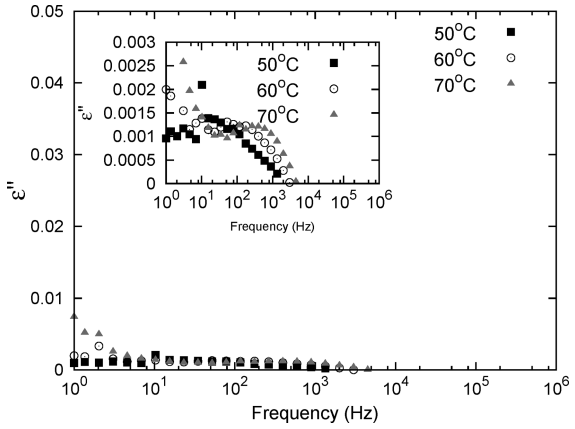

Figure 3. Dielectric loss spectra of mSBR−CB from 50 to 70 °C. There is a weak signal that may correspond to an interfacial relaxation, but it is too weak to analyze and obtain its temperature dependence. Inset shows the same data but with a much smaller *y*-axis range.

Table 3. VFT Fit Parameters for the Interfacial Process of mSBR Composites with Silica and Clay (C20A) and Clay Nanocomposites with PB, SBR5, SBR23, and SBR45 Polymers

	τ_o (s)	B (K)	T_0 (K)
mSBR−C20A	6.79×10^{-6}	61	304
mSBR−silica	3.71×10^{-4}	19	295
PB-C20A	5.10×10^{-8}	364	274
SBR5-C20A	1.85×10^{-6}	127	313
SBR23-C20A	2.50×10^{-7}	380	306
SBR45-C20A	1.02×10^{-6}	111	339

to the concentrations normally used in industry. Figure 3 shows the dielectric loss spectra for mSBR−CB at temperatures where the SBR−filler interfacial mode was observed in Figure 1. A very weak dielectric loss signal is observed in this region, and the position of the peak appears to shift with temperature (see inset of Figure 3 with the same data but smaller *y*-axis range).

However, the signal is just too weak compared to the noise for curve fitting and extrapolation of T_{gi} for this sample. Our measurements are consistent with studies showing that although there is some interaction between carbon black and SBR,[28,29] the interaction is weaker than that of silicates and SBR. There has been speculation that a glassy interphase exists in carbon black−elastomer composites.[19] However, large amounts of carbon black are needed to build the percolating network of glassy interphase and improve the modulus.

All of the results shown thus far contain uncured SBR. To complete the study, cured and uncured (but containing curatives) SBR samples were also tested. Comparison of uncured samples, with or without curing agents, shows that the curatives themselves do not affect either the bulk or the interfacial mode. However, curing does create a difference in bulk polymer relaxation between cured and uncured samples. T_{gb} for uncured mSBR (as extrapolated from dielectric relaxation spectroscopy) is −44 °C, but T_{gb} for cured mSBR is −35 °C. A higher glass transition temperature indicates that the bulk polymer relaxes more slowly in cured samples compared to uncured which is to be expected for cross-linked rubber. Despite the cross-linking, however, the slowed bulk polymer relaxation is still much faster than that of interfacial polymer.

Cross-linking can also affect the interfacial mode. While SBR composites with clay, silica, and carbon black all exhibit a slower relaxation in the uncured state, after curing, only the SBR−clay interfacial mode can be observed. In the cured silica and carbon black composites, the interfacial mode is mostly obscured by the sample conductivity. The heat and shear applied during curing as well as the cross-linking itself better disperses the particles in the matrix, which might lead to increased conductivity. The much weaker signal for the silica and carbon black containing samples accentuates the problem.

While T_{gi} is indicative of interaction strength, the intensity of the dielectric signal partially corresponds to the number of interacting dipoles *provided that there are no differences in any extra correlations between the dipoles* of the interfacial polymer for the three different additives. Therefore, a weaker signal can qualitatively correspond to less interacting polymer compared to a composite with a stronger signal. Because it is difficult to accurately compare the signal strength among different samples (due to, for example, inaccuracies in sample thickness determination), a ratio of the dielectric strength for the interfacial polymer ($\Delta\varepsilon_i$) to the dielectric strength of the bulk polymer ($\Delta\varepsilon_b$) were used to compare the different samples. The interfacial dielectric strength ($\Delta\varepsilon_i$) and bulk dielectric strength ($\Delta\varepsilon_b$) were compared at two different (arbitrary) temperatures, +60 °C and −20 °C, respectively. The dielectric strengths were obtained from fitting the dielectric spectra at these temperatures to the sum of two HN functions and a power law term (see previous discussion) and extracting $\Delta\varepsilon$ from the HN component corresponding to polymer relaxation. We use the ratio of $T_i\Delta\varepsilon_i/T_b\Delta\varepsilon_b$ for each sample as a qualitative indicator of how much of the polymer behaves like the interfacial slow layer compared to that relaxing like the bulk polymer. Table 4 lists the individual $\Delta\varepsilon$ and the ratio $T_i\Delta\varepsilon_i/T_b\Delta\varepsilon_b$ for the clay and silica composites. The signal for the carbon black sample is too weak to analyze quantitatively. The $T_i\Delta\varepsilon_i/T_b\Delta\varepsilon_b$ ratio is three times larger for clay compared to silica. One possible explanation is that the amount of "immobilized" polymer at the interface is higher in the clay-containing sample compared to that with silica or carbon black. Another

Table 4. Interfacial and Bulk Dielectric Strengths Obtained from HN Function Fits to the Dielectric Spectra at +60 and −20°C, Respectively, for Clay and Silica SBR Composites

	$\Delta\varepsilon_i$ (at 60 °C)	$\Delta\varepsilon_b$ (at −20 °C)	$T_i\Delta\varepsilon_i/T_b\Delta\varepsilon_b$
SBR	-	0.00829 ± 0.000 06	-
SBR−clay	0.0378 ± 0.0059	0.00803 ± 0.000 12	6.2
SBR−silica	0.0271 ± 0.0002	0.0152 ± 0.0008	2.3

possibility is that the clay surface aligns the dipoles preferentially (or a combination of both possibilities). Consistent with the first explanation, the immobilized polymer layer near a flat surface (such as, for example, clay) was found to be considerably thicker from that near a curved surface with the same chemistry.[53]

The observed differences in the dielectric behavior attributed to differences in the polymer−filler interactions should affect in an analogous way the macroscopic properties of the (uncured) SBR nanocomposites, i.e., their rheological and mechanical properties. Parts a and b of Figure 4a show the isothermal frequency scans (for temperatures 10 and 100 °C, respectively) for the SBR polymer and its nanocomposites with C20A clay, silica and carbon black. The introduction of all fillers enhances the viscoelastic properties of the matrix; however, the effect is much more pronounced for the clay nanocomposite than for silica and carbon black. Moreover, it is of interest to note that the crossover frequency of the storage and loss modulus (G' and G'', respectively) of both the neat SBR matrix and the SBR−carbon black, observed in Figure 4b, is close to frequency, $\omega = 0.1\ s^{-1}$, but falls outside the rheological window for the clay nanocomposite. The deviations from the ideal melt behavior, mainly in the low frequency limit, and the evolution of a nonterminal mode seen for SBR−clay is a common feature for several classes of nanocomposites;[54−57] this behavior has been attributed to the delayed polymer chain relaxation in the vicinity of the organic/inorganic interface, an effect consistent with the retarded local dynamics observed by dielectric spectroscopy. The dynamic mechanical analysis (DMA) traces of the clay, silica, and carbon black based nanocomposites are compared to the neat matrix in Figure 4c. Apparently, the introduction of clay nanoparticles has a profound impact on the mechanical response of the nanocomposites within the entire temperature range considered, while only a moderate effect can be seen for the SBR−carbon black and SBR−silica composites. A systematic investigation of the mechanical behavior for filled SBR has been report by Berriot et al.[18] Their results have been explained in terms of a gradient of T_g in the vicinity of the filler particles.

The interaction strength of the SBR copolymers with the fillers can be modulated when the composition of the random copolymers, e.g., styrene is systematically altered. Thus, following the investigation of the effect of different fillers on the dynamics of mSBR, composites were studied utilizing a series of SBR copolymers where the amount of styrene was varied; given the strength of the dielectric loss signals, we focused on clay containing nanocomposites. By testing SBR copolymers of different compositions with the same nanoparticles, we can determine how the interfacial polymer relaxation changes as a function of composition and indirectly infer what component of SBR (styrene or butadiene) interacts more strongly with the nanoparticles.

The characteristics of the SBRs used in this section are listed in Table 1. While the polydispersity varies, it is believed that it does

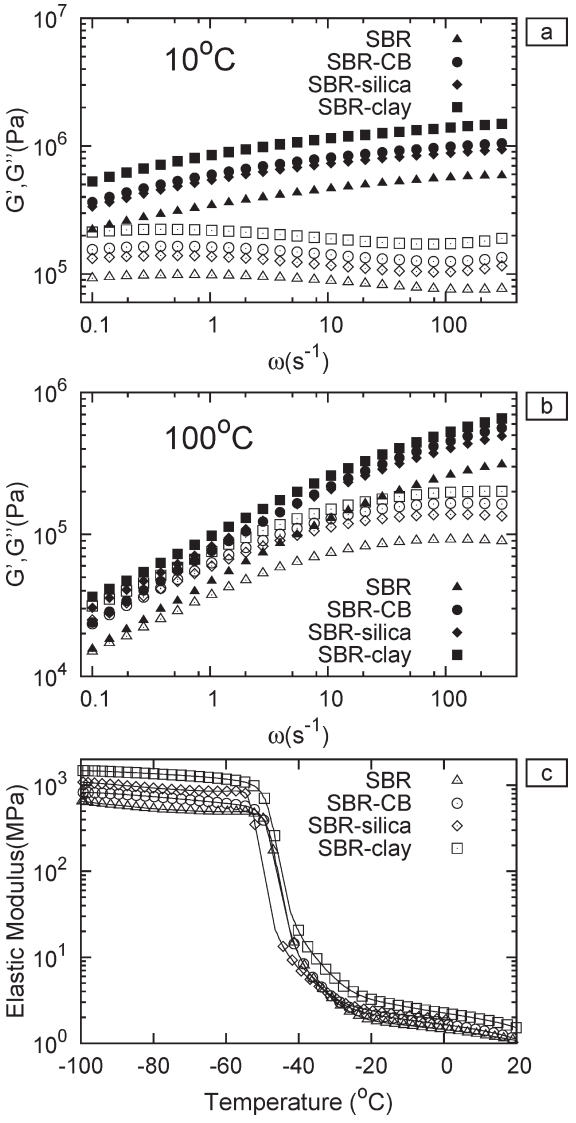

Figure 4. Isothermal frequency scans at temperatures 10 °C (a) and 100 °C (b) for the SBR matrix (triangles), and the SBR−carbon black (circles), SBR−silica (diamonds) and SBR− clay (squares) nanocomposites. Filled symbols correspond to G' and unfilled to G''. (c) DMA traces at 1 Hz of SBR, SBR−carbon black, SBR−silica, and SBR− clay composites.

not adversely affect the measurements. It is well-known that the glass transition temperature does not change significantly with molecular weight above a certain value. For polystyrene, the glass transition temperature plateaus above 21 000 g/mol;[58] gel permeation chromatography (GPC) analysis of this series of copolymers reveal that, despite the high polydispersity, less than 2% of the polymers have molecular weight below 21 000 g/mol. In addition, the dielectric measurements probe only the segmental motion, since polybutadiene does not possess a dipole moment component parallel to the chain backbone. Thus, the measurements follow only the segmental process which is independent of molecular weight. Therefore, polydispersity should not significantly affect comparison of the glass transition temperatures among the different polymers.

The relaxation times, τ, for the interfacial relaxation process for the series of C20A clay nanocomposites are plotted as a

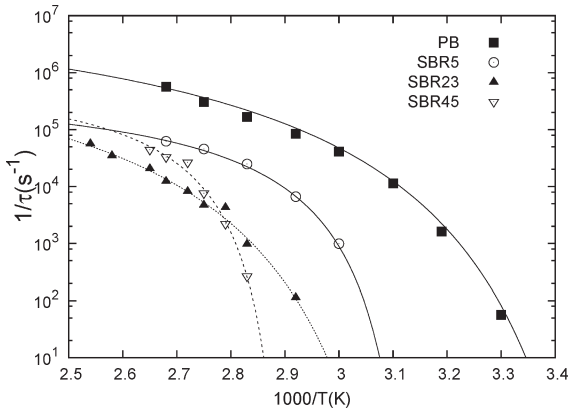

Figure 5. Interfacial relaxation times as a function of temperature for C20A clay composites with SBR polymers of varying styrene content. Lines are VFT (eq 1) fits to the data. Interfacial glass transition temperatures (T_{gi}) are extrapolated from the fits at (τ = 100s). Polybutadiene has the lowest T_{gi} and SBR45 has the highest.

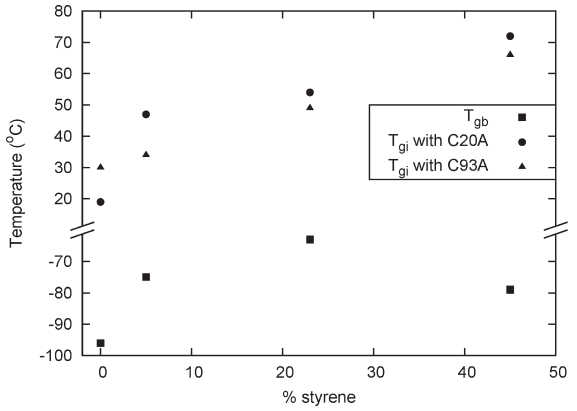

Figure 6. Interfacial and bulk glass transition temperatures for SBRs of varying compositions with 20A and 93A clays. T_{gi} increases as styrene content increases for both 20A and 93A clay, while T_{gb} (as measured by DSC and verified by dielectric relaxation spectroscopy) varies with styrene content within a smaller temperature range. T_{gi} is larger for 20A compared to 93A at every SBR composition.

function of temperature in Figure 5. The relaxation times are fitted to the VFT relation (eq 1) and, from this fit, the interfacial glass transition temperature, T_{gi} is extrapolated for each composite. Note that C20A interacts favorably and is miscible with both polystyrene and polybutadiene homopolymers and all copolymers leading to intercalated nanocomposites. However, as seen in Figure 5 each nanocomposite exhibits a different temperature dependence indicating different interactions with the C20A clay. The extrapolated T_{gi} and T_{gb} for all samples are plotted in Figure 6 as a function of styrene content. The T_{gi} increases as styrene concentration increases and, with the exception of SBR45, so does the bulk T_g. The lowest T_{gi} among this group of polymers corresponds to polybutadiene-C20A with T_{gi} = 19 °C. Even with the lowest T_{gi}, the effective glass transition temperature corresponding to the interfacial polymer is still 115 °C higher than the bulk glass transition temperature of polybutadiene.

Continuing through the composition spectrum, SBR5 copolymer with just 5% styrene exhibits a T_{gi} = 47 °C. Composites with SBR23 and SBR45 containing 23% and 45% styrene, respectively, show interfacial glass transition temperatures of 53 and 73 °C, respectively. While the increases in T_{gi} can be attributed to concomitant increases in the bulk T_g of the polymer we note that the difference between the interfacial and bulk T_g ($T_{gi} - T_{gb}$) also increases as the styrene content increases. We suggest that the trend seen above is due to the styrene interacting more strongly with the clay, more so than butadiene.

Dielectric spectroscopy measures the dipole relaxation of polybutadiene segments, since polystyrene possesses a very weak dipole moment and, thus, its relaxation mode is eclipsed by that of polybutadiene. However, even though only one polymer component (butadiene) is probed, we can indirectly infer the interactions of the other polymer (styrene) because of the macromolecular architecture of the random SBR copolymer. If styrene is being pinned due to strong interactions, butadiene will also "feel" the effects and its relaxation dynamics will be accordingly slowed down. In the case of the C20A nanocomposites, if styrene interacts more strongly with the clay nanoparticles, the dynamics of all segments will slow down as the styrene concentration increases. The strong styrene−clay interaction is due to polar interactions as previously studied though theoretical modeling,[59] and systematic experiments into melt intercalation[60] and intercalation kinetics.[61] We believe butadiene groups also interact favorably but not as strongly as the aromatic (styrene) groups.

In an effort to understand the role of the surface chemistry of the nanoparticles, the results with C20A were compared to a clay modified with a different surfactant, C93A. The surface chemistry of C20A and C93A is very similar except C93A contains a tertiary ammonium while C20A is modified with a quaternary ammonium. The hydrogen in C93A allows the surfactant to hydrogen bond with the oxygen atoms on the silicate surface. This bonding is quite favorable which reduces the surfactant mobility[62] and modifies the surfactant and polymer interactions with the clay. In general, polymer intercalation in organically modified clays is determined by three pairwise interactions:[59] new clay−polymer and surfactant−polymer interactions, which replace clay-surfactant interactions. Polystyrene homopolymer does not intercalate into C93A indicating that the net of the three-way interactions is unfavorable. In contrast, polybutadiene and the series of SBR copolymers do intercalate C93A. We believe the favorable interactions between the butadiene chain and the surfactant molecules[63] contribute to an overall favorable situation leading to polymer intercalation of C93A.

Dielectric relaxation spectroscopy confirm these conclusions. PB/C93A nanocomposites show an interfacial relaxation mode (Figure 6). The extrapolated T_{gi} for this system is 30 °C compared to 19 °C in the case of C20A. Using T_{gi} as a guide, PB seems to interact more strongly with C93A than C20A. Figure 6 also shows the results of C93A with all SBR copolymers. The extrapolated T_{gi} of the copolymers increase as the styrene content increases. However, in contrast to the PB homopolymer, the T_{gi} for C93A are lower compared to the corresponding C20A systems. In addition, there is not a clear trend in the difference between the interfacial and bulk glass transition temperatures ($T_{gi} - T_{gb}$) as a function of styrene content, which first decreases (SBR5 and SBR23) and then increases (SBR45).

It appears that styrene still interacts with C93A even though the favorable interactions are reduced such that polystyrene homopolymer does not intercalate C93A. In SBR, the random copolymer structure allows for the favorable interactions of the

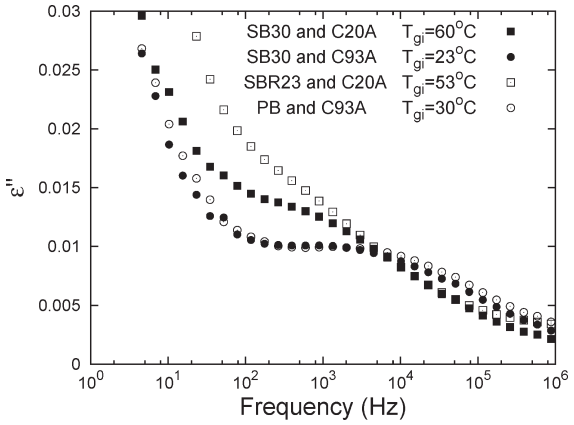

Figure 7. Interfacial relaxation mode at T = 80 °C of SB30 block copolymer with C20A and C93A as well as SBR23 with C20A and PB with C93A for reference. SB30-C20A relaxes more slowly than SB30-C93A. SB30-C20A relaxation more closely resembles that of SBR23-C20A, whereas SB30-C93A more closely resembles PB-C93A.

butadiene segments to bring the styrene segments in close enough proximity to interact with the surface. The interactions with the surface result in higher T_{gi} for SBR−C93A compared to PB-C93A. However, the reduced favorable styrene−silicate interactions of C93A compared to C20A result in lower T_{gi} for SBR copolymer nanocomposites with C93A compared to SBR−C20A nanocomposites.

Finally, both C20A and C93A clays were tested with a polystyrene-*block*-polybutadiene diblock copolymer (SB) to determine the effect of chain architecture. By measuring polymer relaxations, dielectric spectroscopy can also be used to deduce the orientation of one polymer in relation to another polymer in a blend with different structures.[64] The block copolymer used in this study, SB30, contains 30% styrene and it intercalates both C20A and C93A. XRD studies of these nanocomposites show that the clays intercalate to approximately the same interlayer distance with similar structural coherence (same full-width-at-half-maximum of the main diffraction peak). However, even though SB30 intercalates both C20A and C93A, the dielectric spectroscopy reveals very different behavior for the two systems. The interfacial relaxation for SB30-C20A is much slower than that of SB30-C93A (Figure 7). The T_{gi} of SB30-C93A is 23 °C compared to 60 °C for SB30-C20A. In contrast, the T_{gi} for SB30-C20A is similar to the T_{gi} for SBR23-C20A (60 and 53 °C, respectively) indicating that when both components interact favorably with the clay, chain architecture does not affect the segmental dynamics of the interfacial polymer. On the other hand, the T_{gi} for SB30-C93A is much lower; the T_{gi} for SB30-C93A is similar to the T_{gi} for PB-C93A, i.e., 23 and 30 °C, respectively. The similar polymer dynamics for PB-C93A and SB30-C93A indicates that the styrene block in SB30 is not interacting with the C93A surface. The structure of the block copolymer allows the styrene block to avoid the surface whereas the random copolymer structure of SBR brings the styrene segments close to the few available interacting sites at the C93A surface. It is, thus, anticipated that in the region surrounding the clay layers, the block copolymer is likely oriented so that the polybutadiene block is at the surface while the polystyrene block is away from the surface (i.e., toward the bulk). The chain structure can even allow for block separation between the layers; simulations on block copolymer nanocomposites reveal that when one block does not interact favorably with the clay surface, it is intercalated but remains in the middle of the gallery while the favorable block resides more closely at the clay surface.[65]

CONCLUDING REMARKS

Dielectric relaxation spectroscopy was used to measure polymer dynamics in SBR and SBR nanocomposites. Both the bulk and interfacial polymer relaxations were measured and quantified by the glass transition temperatures associated with the polymer relaxation. The interfacial polymer relaxed much more slowly than the bulk polymer due to its favorable interactions with the nanoparticle surface. SBR was tested with different fillers including clay, silica, and carbon black. All three composites exhibited a slower interfacial relaxation. The interfacial glass transition for mSBR−clay nanocomposites is more than 80 °C higher than the bulk SBR glass transition temperature. The interfacial glass transition temperature of SBR−silica was about 65 °C higher than the bulk T_g. The interfacial polymer in the SBR−clay nanocomposite relaxes more slowly than in SBR−silica nanocomposite indicating stronger interactions between SBR and clay. A very weak secondary interfacial relaxation mode was observed for SBR−carbon black composites that could not be analyzed quantitatively. The interfacial relaxation mode in SBR−clay is strong even after cross-linking. Cross-linking enhances the conductivity in silica and carbon black samples which eclipses the interfacial relaxation mode in those samples.

Clay nanocomposites with SBRs of different compositions were also tested. In the case of C20A, where both polystyrene and polybutadiene homopolymers interact favorably and intercalate the clay, polymer dynamics became slower as the styrene concentration increased indicating that styrene interacts more strongly with clay than the butadiene. Butadiene groups also interact favorably with clay but not as strongly as the aromatic (styrene) groups.

On the other hand, polystyrene does not interact as strongly with C93A and it does not intercalate within C93A, but SBR copolymers do intercalate within C93A due to additional favorable polybutadiene−C93A interactions. In the case of the random copolymers, the styrene segments are brought in proximity to the silicate surface with which they interact favorably. Nanocomposites of C20A with polystyrene−polybutadiene block copolymers exhibit similar interfacial polymer dynamics with nanocomposites based on SBR random copolymers (of similar composition) despite the different polymer architecture. Polymer dynamics of polystyrene-polybutadiene block copolymer with C93A more closely resembles that of C93A−polybutadiene nanocomposite, which indicates that the block structure of the diblock allows the styrene block to avoid interaction with C93A.

ASSOCIATED CONTENT

Supporting Information. Comparison of dispersion (TEM) and dielectric strength of clay, silica and carbon black filled SBR samples. This material is available free of charge via the Internet at http://pubs.acs.org/.

AUTHOR INFORMATION

Corresponding Author
*E-mail: epg2@cornell.edu.

■ ACKNOWLEDGMENT

This publication is based on work supported in part by Award No. KUS-C1-018-02, made by King Abdullah University of Science and Technology. Additional support was provided by Michelin under the guidance of Julie McCormick, Stephanie Nesbitt, and Aiying Wang. L.V. also gratefully acknowledges support from the NSFGRP fellowship. This work made use of the Cornell Center for Materials Research Experimental Facilities. S.H.A. would like to acknowledge that part of this research was sponsored by the Greek General Secretariat of Research and Technology (ΠΕΝΕΔ 2003 programme, project 03ΕΔ581) and by the European Union (STREP Programme, project NMP3-CT-2005-506621). We thank Haris Retsos for his contribution to the initial work in dielectric spectroscopy, Antonios Kelarakis for his work on rheological and DMA measurements, and Luis Estevez for his work in TEM imaging. We also thank Richard Vaia and Creighton Thomas for helpful discussions.

■ REFERENCES

(1) O'Haver, J. H.; Harwell, J. H.; Evans, L. R.; Waddell, W. H. *J. Appl. Polym. Sci.* **1996**, *59*, 1427–1435.
(2) Zhou, Z.; Liu, S.; Gu, L. *J. Appl. Polym. Sci.* **2001**, *80*, 1520–1525.
(3) Nair, K. G.; Dufresne, A. *Biomacromolecules* **2003**, *4*, 666–674.
(4) Bokobza, L. *Polymer* **2007**, *48*, 4907–4920.
(5) Usuki, A.; Tukigase, A.; Kato, M. *Polymer* **2002**, *43*, 2185–2189.
(6) Arroyo, M.; Lopez-Manchado, M. A.; Herrero, B. *Polymer* **2003**, *44*, 2447–2453.
(7) Okada, A.; Usuki, A.; Kurauchi, T.; Kamigaito, O.; *ACS Symposium Series: Hybrid Organic-Inorganic Composites*; Mark, J. E., Lee, C. Y. C., Bianconi, P. A., Eds.; American Chemical Society: Washington, DC, 1995.
(8) Bala, P.; Samantaray, B.; Srivastava, S.; Nando, G. *J. Appl. Polym. Sci.* **2004**, *92*, 3583–3592.
(9) Song, M.; Wong, C. W.; Jin, J.; Ansarifar, A.; Zhang, Z. Y.; Richardson, M. *Polym. Int.* **2005**, *54*, 560–568.
(10) Sadhu, S.; Bhowmick, A. K. *J. Polym. Sci., Part B: Polym. Phys.* **2004**, *42*, 1573–1585.
(11) Ma, J.; Xiang, P.; Mai, Y.; Zhang, L. *Macromol. Rapid Commun.* **2004**, *25*, 1692–1696.
(12) Wang, M. J. *Rubber Chem. Technol.* **1998**, *71*, 520–589.
(13) Kaufmann, S.; Slichter, W. P.; Davis, D. D. *J. Polym. Sci., Part A-2* **1971**, *9*, 829–839.
(14) Landry, C. J. T.; Coltrain, B. K.; Landry, M. R.; Fitsgerald, J. J.; Long, V. K. *Macromolecules* **1993**, *26*, 3702–3712.
(15) Kim, J. S.; Jackman, R.; Eisenberg, A. *Macromolecules* **1994**, *27*, 2789–2803.
(16) Tsagaropoulos, G.; Eisenberg, A. *Macromolecules* **1995**, *28*, 396–398.
(17) Tsagaropoulos, G.; Eisenberg, A. *Macromolecules* **1995**, *28*, 6067–6077.
(18) Berriot, J.; Montes, H.; Lequeux, F.; Long, D.; Sotta, P. *Macromolecules* **2002**, *35*, 9756–9762.
(19) Merabia, S.; Sotta, P.; Long, D. R. *Macromolecules* **2008**, *41*, 8252–8266.
(20) Chen, L.; Zheng, K.; Tian, X.; Hu, K.; Wang, R.; Liu, C.; Li, Y.; Cui, P. *Macromolecules* **2010**, *43*, 1076–1082.
(21) Keddie, J. L.; Jones, R. L.; Cory, R. A. *Faraday Discuss* **1994**, *98*, 219–230.
(22) Van Zanten, J. H.; Wallace, W. E.; Wu, W. *Phys. Rev. E* **1996**, *53*, R2053–R2056.
(23) Alcoutlabi, M.; McKenna, G. B. *J. Phys.: Condens. Matt.* **2005**, *17*, R461–R524.
(24) Roth, C. B.; Dutcher, J. R. *J. Electroanal. Chem.* **2005**, *584*, 13–22.
(25) Bansal, A.; Yang, H.; Li, C.; Cho, K.; Benicewicz, B. C.; Kumar, S. K.; Schadler, L. S. *Nat. Mater.* **2005**, *4*, 693–698.
(26) Vo, L. T.; Giannelis, E. P. *Macromolecules* **2007**, *40*, 8271–8276.
(27) Chen, H.; Schmidt, D. F.; Pitsikalis, M.; Hadjichristidis, N.; Zhang, Y.; Wiesner, U.; Giannelis, E. P. *J. Polym. Sci., Part B: Polym. Phys.* **2003**, *41*, 3264–3271.
(28) Kraus, G.; Dugone, J. *Ind. Eng. Chem.* **1955**, *47*, 1809–1816.
(29) Dutta, N.; Choudhury, N.; Haidar, B.; Vidal, A.; Donnet, J.; Delmotte, L.; Chezeau, J. *Polymer* **1994**, *35*, 4293–4299.
(30) Berriot, J.; Lequeux, F.; Monnerie, L.; Montes, H.; Long, D.; Sotta, P. *J. Non-Cryst. Solids* **2002**, *307−310*, 719–724.
(31) Berriot, J.; Martin, F.; Montes, H.; Monnerie, L.; Sotta, P. *Polymer* **2003**, *44*, 1437–1447.
(32) Arrighi, V.; McEwen, I. J.; Qian, H.; Serrano Prieto, M. B. *Polymer* **2003**, *44*, 6259–6266.
(33) Alternatively, the data can be fitted quite well to a sum of a power law conductivity term and two log-normal functions. The log-normal distributions fit well the interfacial polymer relaxation and give relaxation times that are within less than 20% of the relaxation times calculated using two HN functions. The relaxation times from the log-normal function analysis are used in Figures 2 and 4 because such fit requires fewer adjustable parameters.
(34) DSC measurements do not show any step in the heat capacity curve in the temperature range of this "effective glass transition temperature" of the slow interfacial dynamics, so it cannot be really assigned to a glass transition associated with segmental relaxation.
(35) Hernadez, M.; Carretero-Gonzalez, J.; Verdejo, R.; Ezquerra, T. A.; Lopez-Manchado, M. A. *Macromolecules* **2010**, *43*, 643–651.
(36) Xu, W.; Raychowdhury, S.; Jiang, D. D.; Retsos, H.; Giannelis, E. P. *Small* **2008**, *4*, 662–669.
(37) Carretero-Gonzalez, J.; Retsos, H.; Giannelis, E. P.; Ezquerra, T. A.; Hernandez, M.; Lopez-Manchado, M. A. *Soft Matter* **2009**, *5*, 3481–3486.
(38) Mischer, C.; Baschnagel, J.; Binder, K. *Adv. Colloid. Interf. Sci.* **2001**, *94*, 197.
(39) Baschnagel, J.; Varnik, F. *J. Phys.: Condens. Matt.* **2005**, *17*, R851–R953.
(40) Vaia, R. A.; Sauer, B. B.; Tse, O. K.; Giannelis, E. P. *J. Polym. Sci., Part B: Polym. Phys.* **1997**, *35*, 59–67.
(41) Anastasiadis, S. H.; Karatasos, K.; Vlachos, G.; Manias, E.; Giannelis, E. P. *Phys. Rev. Lett.* **2000**, *84*, 915–918.
(42) Manias, E.; Kuppa, V.; Yang, D. K.; Zax, D. B. *Colloids Surf., A* **2001**, *187−188*, 509–521.
(43) Lu, H.; Nutt, S. *Macromolecules* **2003**, *36*, 4010–4016.
(44) Bohning, M.; Goering, H.; Fritz, A.; Brzezinka, K.-W.; Turky, G.; Schönhals, A.; Schartel, B. *Macromolecules* **2005**, *38*, 2764–2774.
(45) Mijovic, J.; Lee, H. K.; Kenny, J.; Mays, J. *Macromolecules* **2006**, *39*, 2172–2182.
(46) Elmahdy, M. M.; Chrissopoulou, K.; Afratis, A.; Floudas, G.; Anastasiadis, S. H. *Macromolecules* **2006**, *39*, 5170–5173.
(47) Chrissopoulou, K.; Afratis, A.; Anastasiadis, S. H.; Elmahdy, M. M.; Floudas, G.; Frick, B. *Eur. Phys. J.—Spec. Top.* **2007**, *141*, 267–271.
(48) Chrissopoulou, K. S. H.; Anastasiadis, S. H.; Giannelis, E. P.; Frick, B. *J. Chem. Phys.* **2007**, *127*, 144910.
(49) Fotiadou, S.; Chrissopoulou, K.; Frick, B.; Anastasiadis, S. H. *J. Polym. Sci., Part B: Polym. Phys.* **2010**, *48*, 1658–1667.
(50) Ngai, K. L. *Philos. Mag. B* **2002**, *82*, 291–303.
(51) Adam, G.; Gibbs, J. H. *J. Chem. Phys.* **1965**, *43*, 139.
(52) Donth, E. *The Glass Transition*; Springer: Berlin, 2001.
(53) Harton, S. E.; Kumar, S. K.; Yang, H.; Koga, T.; Hicks, K.; Lee, H.; Mijovic, J.; Liu, M.; Vallery, R. S.; Gidley, D. W. *Macromolecules* **2010**, *43*, 3415–3421.
(54) Krishnamoorti, R.; Yurekli, K. *Curr. Opin. Colloid Interface Sci.* **2001**, *6*, 464–470.
(55) Kelarakis, A.; Yoon, K.; Somani, R. H.; Chen, X. M.; Hsiao, B. S.; Chu, B. *Polymer* **2005**, *46*, 11591–11599.
(56) Kelarakis, A.; Giannelis, E. P.; Yoon, K. *Polymer* **2007**, *48*, 7567–7572.
(57) Tjong, S. C. *Mater. Sci. Eng. R-Rep.* **2006**, *53*, 73–197.

(58) Claudy, P.; Letoffe, J. M.; Camberlain, Y.; Pascault, J. P. *Polym. Bull.* **1983**, *9*, 208–215.
(59) Vaia, R. A.; Giannelis, E. P. *Macromolecules* **1997**, *30*, 7990–7999.
(60) Vaia, R. A.; Giannelis, E. P. *Macromolecules* **1997**, *30*, 8000–8009.
(61) Manias, E.; Chen, H.; Krishnamoorti, R.; Genzer, J.; Kramer, E. J.; Giannelis, E. P. *Macromolecules* **2000**, *33*, 7955–7966.
(62) Heinz, H.; Vaia, R. A.; Krishnamoorti, R.; Farmer, B. L. *Chem. Mater.* **2007**, *19*, 59–68.
(63) Tausendfreund, I.; Bandermann, F.; Siesler, H. W.; Kleimann, M. *Polymer* **2002**, *43*, 7085–7091.
(64) Fragiadakis, D.; Runt, J. *Macromolecules* **2010**, *43*, 1028–1034.
(65) Shah, D.; Bitsanis, A.; Natarajan, U.; Hackett, E.; Giannelis, E. P. *Mater. Res. Soc. Symp. Proc.* **2002**, *773E*, T1.1.1–T1.1.11.